15 May 2002

ELSEVIER

Optics Communications 206 (2002) 141–147

OPTICS COMMUNICATIONS

www.elsevier.com/locate/optcom

Two-dimensional atomic interferometry for creation of nanostructures

Y. Tan, J. Morzinski, A.V. Turukhin, P.S. Bhatia *, M.S. Shahriar

Research Laboratory of Electronics, Massachusetts Institute of Technology, Cambridge, MA 01239, USA

Received 14 November 2001; received in revised form 16 January 2002; accepted 23 January 2002

Abstract

We propose a scheme for large angle two-dimensional atom interferometers employing two-photon pulses. The interferometer scheme utilizes Raman pulses to produce a two-dimensional pattern with independent choice of grating spacings in each direction, each being as small as 2 nm. This scheme may enable one to produce uniform arrays of structures such as quantum dots with dimensions of only a few nm on each side. © 2002 Published by Elsevier Science B.V.

PACS: 07.10.Yg; 03.75.Dg; 07.60.Ly; 42.50.Vk

In recent years, rapid progress has been made in the area of atom interferometry. Sensitivity of the modern atomic beam gyroscopes is exceeding that of ring laser gyroscopes [1,2]. Atom interferometers have been used to precisely measure the ratio of Planck's constant to atomic mass, acceleration due to gravity, as well as the gradient thereof [3,4]. Rotation sensors based on atom interferometry may enable measurement of general relativistic Lens–Thirring rotation in the near future. For nano-technology an atom interferometer with a high coherence-length source of atoms, such as the Bose-condensed atom laser [5], would enable the creation of one- and two-dimensional structures with feature sizes of less than 10 nm. For both scientific and technological applications, the sensitivity of an atom interferometer is proportional to the area enclosed by the different paths, which in turn is determined by the degree of splitting at the input port. For the current schemes, the achievable splitting is limited to a few photon recoils. To further increase sensitivity of an atom interferometer, much larger splitting angle is required.

Several schemes of large angle atom cloud splitters have been studied. The interaction of a two level atom with a standing wave light field can produce large splitting angles, but the atoms are scattered into multiple orders [6] because of the sinusoidal nature of the phase grating. The magneto-optic beam-splitter [7–9] and variations thereof [10–12] produce a triangular phase grating, which represents an improvement over the pure standing wave. However, the number of higher

* Corresponding author. Fax: +1-617-253-6412.
E-mail address: psbhatia@mit.edu (P.S. Bhatia).

0030-4018/02/$ - see front matter
PII: S0030-4018(02)01365-2

orders is still significant because of the sub-wavelength extent of the triangular shapes. In addition, all of these schemes involve an optical interaction with the excited state of the atom and, therefore, suffer from the decoherence effects. In order to minimize these effects, the interaction time has to be small compared to the natural lifetime. This in turn limits the maximum coherent splitting to less than 20 photon recoils due to constraints imposed by high frequency modulators.

In this paper, we consider a beam splitter which can achieve a splitting exceeding ± 100 photon recoils. Originally suggested independently by us [13] and McGuirk et al. [14], a version of this splitter has recently been demonstrated experimentally [14]. Here, we show how this approach can be extended to realize a high-sensitivity interferometer in two-dimensions. The ability of the scheme to generate real two-dimensional interference patterns might be used for lithographic applications such as production of arrays of quantum dots. As an example, we consider the ^{87}Rb atom, released from an evaporatively cooled magnetic trap (or a Bose condensate) and falling under gravity. The relevant energy levels are shown in Fig. 1. The atoms are assumed to be in state $|F = 1, m_f = 1\rangle$ at the onset. We excite the Raman transition, coupling $|F = 1,\ m_f = 1\rangle$ (hereafter referred to as $|a\rangle$) to $|F = 2,\ m_f = 1\rangle$ (hereafter referred to as $|c\rangle$). The beams are detuned strongly from the excited manifold of the D_2 line, but are two-photon-resonant, so that the process can be thought of as a two-level transition between the two magnetic sublevels. Here, the quantization direction, **z**, is assumed to be normal to the direction of gravity, denoted as **y**.

We assume that right after the atoms are released from their trap, they are in state $|a, p_z = 0,\ p_x = 0\rangle \equiv |a, 0, 0\rangle$. We apply two right circularly (σ^+) polarized beams which are counter-propagating along the **z** axis, with frequencies chosen so one beam (hereafter called A) couples $|a\rangle$ to the excited state, while the other beam (hereafter called C) couples $|c\rangle$ to the same excited state. Both beams are pulsed, with pulse timing chosen so that counter-propagating pulses arrive at the atom simultaneously and leave the atom simultaneously. In our scheme, the first pulse's duration is chosen so that the pulse is a $\pi/2$-pulse, with beam A propagating in the $-\mathbf{z}$ direction and beam C propagating in the $+\mathbf{z}$ direction, so that the effect is to place the atom in an equal superposition of $|a, 0, 0\rangle$ and $|c, -2\hbar k, 0\rangle$. This is illustrated in Fig. 2 (solid line transitions). The

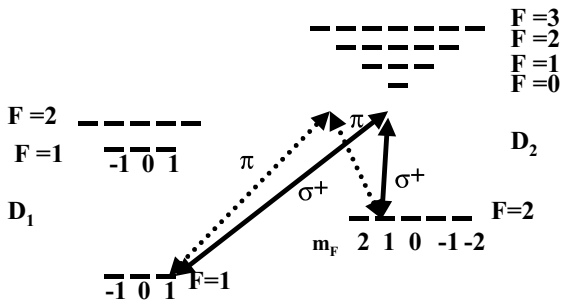

Fig. 1. The relevant energy levels of ^{87}Rb atoms (not to scale). Transitions from the D_2 manifolds are used. The presence of two different types of Raman transitions in the D_2 manifold, excitable by optical beams propagating in orthogonal direction, is a key element of this design. Note that because of the particular magnetic sublevels chosen as $|a\rangle$ and $|c\rangle$, both σ_+–σ_- as well as π–π Raman transition exist for coupling these two states. This, for example, is not the case if $m_f = 0$ levels were chosen for both $|a\rangle$ and $|c\rangle$, because of selection rules prohibiting $\Delta f = 0$, $\Delta m_f = 0$ transitions, and the constraint that $|\Delta f| \leqslant 1$.

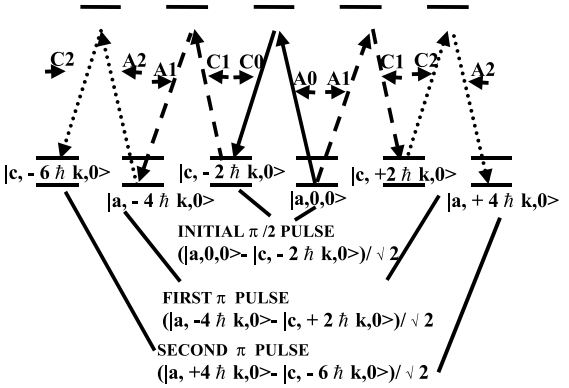

Fig. 2. Schematic illustration of the first three pulses in the Raman pulse beamsplitter. Explicit form of the initial superposition state, after excitation with the $\pi/2$-pulse, is shown along with the superposition states resulting after the first and second π-pulses are applied. Solid lines denote transitions excited with the $\pi/2$-pulse, dashed lines denote the first π-pulse, dotted lines denote the second π-pulse. Note that the π-pulses excite two Raman transitions in parallel. Momentum selection rules ensure that there is no mixing of these transitions. For clarity, the energy shifts due to kinetic energy are omitted.

second pulse pair has a longer duration, chosen so that it acts as a π-pulse, and also has the directions of beams A and C exchanged. This will cause a π-pulse transition between states $|a\rangle$ and $|c\rangle$, and the reversal of the beam direction will transfer $|a,0,0\rangle$ to $|c,+2\hbar k,0\rangle$ and $|c,-2\hbar k,0\rangle$ to $|a,-4\hbar k,0\rangle$ (dashed-line transitions in Fig. 2). Note that the π-pulses excite two Raman transitions in parallel, that momentum selection rules ensure that there is no mixing of these transitions, and that the atoms are still in an equal superposition of two states. The third pulse pair has the same duration as the second (i.e., it excites a π-pulse transition), but the directions of A and C are again exchanged. The state of the atom after this second π-pulse will now be an equal superposition of $|a,+4\hbar k,0\rangle$ and $|c,-6\hbar k,0\rangle$ (dotted-line transitions in Fig. 2). Each subsequent pair of π-pulses again exchanges the directions of A and C, driving the atomic superposition to larger momentum splittings. After exposure to an even number N_z of these alternating-direction pairs of π-pulses, the atoms will be in an equal superposition of states $|a,+2N_z\hbar k,0\rangle$ and $|c,-(2N_z+2)\ \hbar k,0\rangle$.

For example, $N_z = 24$ alternating-pulses will put the atoms in a superposition of states $|a,+48\hbar k,0\rangle$ and $|c,-50\hbar k,0\rangle$. The p_z difference of $98\hbar k$ corresponds to a velocity of about 0.6 m/s, and after 3.3 ms the atoms will separate into two clouds with a spatial separation of 2 mm. We can now reverse the motion of the clouds by reversing the splitting scheme and then continue to exchange pulse directions each time a π-pulse exchanges the atomic states. $N_z = 24$ of these reversed pulses would bring the atoms back to the equal superposition of $|a,0,0\rangle$ and $|c,-2\hbar k,0\rangle$, and a further 25 pulses (for a total of 49) would put the atoms in a superposition of states $|c,-50\hbar k,0\rangle$ and $|a,+48\hbar k,0\rangle$, moving the two halves of the cloud back towards each other.

While the spatially separated components of the superposition state are moving toward each other, we can apply a pair of linearly π polarized beams, co-propagating along the **x** direction, causing a Raman transition between $|a\rangle$ and $|c\rangle$ (dotted-line transitions in Fig. 1). The duration of this pulse pair is chosen such that a π-pulse is induced on the two-photon transition coupling $|a\rangle$ and $|c\rangle$, and the location of the beam is chosen so that it only affects the component of the cloud that corresponds to the state $|c,-50\hbar k,0\rangle$. The atom is now in an equal superposition of the states $|a,-50\hbar k,0\rangle$ and $|a,+48\hbar k,0\rangle$, since the co-propagating fields give no net momentum transfer in the **x** direction. If left alone these components will come together in about 3.3 ms and form fringes with a peak-to-peak spacing of about 8 nm. But before that happens we can split (and later recombine) each component further along the **x** axis. We will use a pair of linearly polarized beams with frequencies A and C, counter-propagating in the **x** direction. In a manner analogous to the **z** directed splitting, we first apply a π/2-pulse, interacting with both components of the split cloud, which produces an equal superposition of four states: $\{|a,-50\hbar k,0\rangle, |c,\ -50\hbar k,-2\hbar k\rangle\}$ separated spatially in the **z** direction from $\{|a,48\hbar k,0\rangle,\ |c,\ 48\hbar k,-2\hbar k\rangle\}$. This is followed by a series of N_x direction-alternating π-pulse pairs, producing a set of four states. For even N_x, the states are

$$\{|a,-50\hbar k,2N_xk\rangle,|c,-50\hbar k,-(2N_x+2)k\rangle\}$$
$$\text{and}\quad \{|a,48\hbar k,2N_xk>,|c,48\hbar k,-(2N_x+2)\hbar k\rangle\}.$$

The two clouds in curly brackets are spatially separate from each other in the **z** direction, while inside each cloud two subclouds will now separate out in the **x** direction, with a velocity of 1.2 m/s if $N_x = 2N_z = 48$. Thus, after about 1.7 ms, the separation in the **x** direction will be about 2 mm in each cloud. At this point, $2N_x + 1 = 97$ π-pulses will be applied in the **x** direction, with the pulse directions chosen to reverse the momentum splitting in the **x** direction. This will produce an equal superposition of the four states:

$$\{|a,-50\hbar k,-98\hbar k\rangle,|c,-50\hbar k,96\hbar k\rangle\}$$
$$\text{and}\quad \{|a,48\hbar k,-98\hbar k\rangle,|c,48\hbar k,96\hbar k\rangle\}.$$

When these states merge their interference fringe spacing would be on the order of a few nanometers, which would be difficult to detect by optical grating diffraction. To observe the interference and optimize the amplitude in real time, we could scan the phase of one of the laser pulses and detect the atoms either in state $|a\rangle$ or in state $|c\rangle$. The population in either state is a function of the optical phase scan. Note that this phase-scan interference pattern can be observed without resolving the spatial interference pattern.

Finally, after optimizing the phase-scan interference pattern, a **z** directed pair of copropagating, circularly polarized beams are now used to excite a π transition between $|a\rangle$ and $|c\rangle$, but located spatially so as to affect only the $|c\rangle$ subcloud of each **z** separated cloud. The separation of 2 mm in the **x** direction makes this selective excitation possible. After this pulse sequence, we have four subclouds, converging toward one another in both **x** and **z** directions, and each in the internal state $|a\rangle$:

$$\{|a,-50\hbar k,-98\hbar k\rangle,|a,-50\hbar k,96\hbar k\rangle\}$$

and $\{|a,48\hbar k,-98\hbar k\rangle,|a,48\hbar k,96\hbar k\rangle\}$.

Note that the subclouds are now separated in the **z** direction by 1 mm, and in the **x** direction by 2 mm. Similarly, the speed of convergence in the **z** direction (about 0.6 m/s) is half of the convergence speed in the **x** direction. As such, all four components of the cloud will come together in another 1.7 ms, forming a two-dimensional matter wave grating pattern. The spacing of these patterns are determined by the values of N_z and N_x: for the rubidium transition wavelength of about 800 nm, the peak-to-peak separation in the **z** direction is approximately $100/N_z$ nm, and the separation in the **x** direction is $100/N_x$ nm. For the parameters chosen here, we would have a grating with about 4 nm spacing in the **x** direction, and 8 nm spacing in the **z** direction. Structures as small as 2 nm seem feasible given the source particles' parameters considered here. For lithographic applications, this pattern can be deposited on a substrate coated with self-assembled monolayers of octyltrichlorosilane. Then, the damage induced on this layer can be transferred chemically to an underlying layer of semiconductors or coinage metals [15]. The number of spots, and uniformity of height thereof, are determined largely by the coherence length of the sample. For a Bose condensed source, the coherence length is of the order of 300 μm, so that up to 10^{10} structures can be produced and deposited over an area of 300 μm diameter.

One of the potential constraints of this approach is the detuning resulting from the Doppler shift of the components of the atomic wave packet with a high transverse momentum. In practice, the maximum detuning that can be tolerated is limited by the available Rabi frequency. In what follows, we consider an explicit example to illustrate the limit involved.

The Raman coupling between $|a,p\rangle$ and $|b,p\pm 2\hbar k\rangle$, for example, suffers from a detuning given by

$$\Delta=[(p\pm 2\hbar k)^2-p^2]/2m\hbar=\pm\frac{2pk}{m}+\frac{2\hbar k^2}{m}.$$

The last term is the same for all p, and can be accounted for by tuning the laser frequencies appropriately. The first term is the Doppler shift:

$$\Delta_d=\pm\frac{2kp}{m}.$$

In our model, the maximum value of p we have contemplated is $\approx 100\hbar k$, so that

$$|\Delta_d|_{\max}=200\frac{\hbar k^2}{m}=200\omega_R,$$

where ω_R is the single photon recoil frequency which, for the ^{87}Rb transition considered is $\approx 2\pi\times 4\times 10^3\ \mathrm{s}^{-1}$. Therefore, $|\Delta_d|_{\max}\cong 2\pi\times 1.6\times 10^6\ \mathrm{s}^{-1}\approx 0.3\Gamma$, where Γ is the population decay rate of the states that are excited by the single frequency transitions. In order to ensure that this detuning does not affect the efficiency of the transition significantly, one must use a Raman (i.e., two-photon) Rabi frequency that is much larger.

Explicitly, let us assume that the smallest spot size for the optical beams is about 10 μm. If a Ti:Sapphire laser is used along with acousto-optic modulators, it is possible to have ~500 mW for each of the single frequency transitions. The strongest of the atomic transitions that are allowed in the level structure shown in Fig. 1 have a saturation intensity of about 3 mW/cm^2. Allowing for the fact that some transition are about a factor of 4 weaker, we assume a saturation intensity of 12 mW/cm^2. This implies that

$$\frac{I_{\max}}{I_{\mathrm{sat}}}\approx\left(\frac{500\ \mathrm{mW}}{(10\ \mu\mathrm{W})^2}\right)\Big/(12\ \mathrm{mW/cm^2})$$
$$=40\times 10^6\ \Rightarrow\ \frac{\Omega_{\max}}{\Gamma}=\sqrt{\frac{I}{I_{\mathrm{sat}}}}\approx 6\times 10^3$$
$$\Rightarrow\ \Omega_{\max}\approx 6\times 10^3\Gamma,$$

where Ω is the Rabi frequency for a single-frequency transition. Of course, the relevant parameter is the Raman Rabi frequency, which is given by

$$\Omega_R \approx_1 \times \frac{\Omega_1 \Omega_2}{\delta} \approx \frac{\Omega_0^2}{\delta} \quad (\text{Assuming, } \Omega_1 \approx \Omega_2 = \Omega_0),$$

Where Ω_1 and Ω_2 are the Rabi frequencies for the two single frequency transitions, and δ is the single photon detuning. In order to ensure that spontaneous emission remains negligible, we want

$$\left(\frac{\Omega_0}{\delta}\right)^2 \times \Gamma \times \tau \ll 1 \quad (\text{Assuming } \Omega_0 \ll \delta)$$
$$\Rightarrow \quad \Omega_R \times \frac{\Gamma}{\delta} \times \tau \ll 1$$
$$\Rightarrow \quad \Omega_R \times \tau \ll \frac{\delta}{\Gamma},$$

where τ is the interaction time. For concreteness, we assume $\delta = 1000\Gamma$ (i.e., about 5 GHz), so that $\Omega_R \tau \ll 1000$. For this choice of δ, and assuming $\Omega_0 = 100\Gamma$ (which is easily possible, given that the maximum achievable value is 6000Γ, as shown above, and satisfies the condition that $\Omega_0 \ll \delta$), we get

$$\Omega_R \approx \frac{\Omega_0^2}{\delta} \approx \frac{(100\Gamma)^2}{100\Gamma} \approx 10\Gamma.$$

To ensure a π-pulse during each Raman pulse, we want $\Omega_R \tau \approx 50\pi$ which satisfies the constraint determined above. The individual pulse duration is

$$\frac{\tau}{50} \approx \frac{\pi}{\Omega_R} \approx \frac{\pi}{10\Gamma} = 10 \text{ ns}.$$

Such a pulse duration can be easily achieved experimentally, using Pockel cells, for example.

In the discussion above, we considered only the state with zero initial momentum. To see the effect of wave packet evolution on the interference pattern, we start with a Gaussian wave packet and Fourier transform it into momentum space. We take into account the initial momentum in the **x** and **z** directions and average the interference process over the initial wave packet. Fig. 3 shows schematically the steps involved in producing the two-dimensional beam-splitting and recombining. At point S, right after atoms are released from the trap, assume the initial momentum state is $|\Psi_0\rangle = |a, p_{ox}\hbar k, p_{oz}\hbar k\rangle$. In what follows, we assume that the duration of the interaction with the laser pulses is negligible compared to the free evolution time of the wave-packet. Components of the wave-packet following the four distinct paths S–A–A1–E, S–A–A2–E, S–B–B1–E and S–B–B2–E will accumulate different phase factors resulting from the distinct kinetic energy along each path. We denote these phase factors as α_1, α_2, α_3 and α_4 respectively. At point E, the momentum state then becomes:

$$\begin{aligned}|\phi 1(p_{ox}, p_{oz})\rangle = 1/2 \quad & (\alpha_1 |a, (p_{oz} + 2N_z - 2)\hbar k, \\ & (p_{ox} - 2N_x)\hbar k\rangle + \alpha_2 |a, \\ & (p_{oz} + 2N_z - 2)\hbar k, \\ & (p_{ox} + 2N_x - 2)\hbar k\rangle + \alpha_3 |a, \\ & (p_{oz} - 2N_z)\hbar k, \\ & (p_{ox} - 2N_x)\hbar k\rangle + \alpha_4 |a, \\ & (p_{oz} - 2N_z)\hbar k, \\ & (p_{ox} + 2N_x - 2)\hbar k\rangle).\end{aligned}$$

The whole wave packet at E is then given by summing over the initial spread in momentum in x and z direction:

$$|\varphi\rangle = \int\int \mathrm{d}p_{ox}\, \mathrm{d}p_{oz} \frac{2\delta}{\sqrt{2\pi}} \times \exp[-\delta^2 (p_{ox}^2 + p_{oz}^2) k^2]^* |\varphi(p_{ox}, p_{oz})\rangle,$$

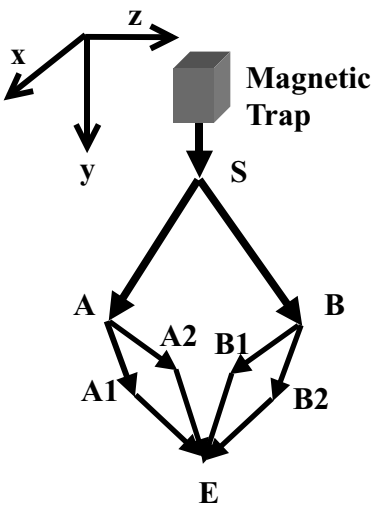

Fig. 3. An illustration of the steps involved in producing two-dimensional beam-splitting and recombining. For simplicity, the laser beams are not shown in the diagram.

where δ is the standard deviation of the initial packet in position space. The interference pattern is given by $P(x,z) \equiv \psi(x,z)^* \psi(x,z)$, where $\psi(x,z) = \langle a,z,x|\varphi\rangle$ is the spatial wave function. We get:

$$P(x,z) = \frac{4}{2\pi(\delta^2 + (\hbar^2 t^2/m^2\delta^2))} \cos^2[(2N_z+1)kz] \times \cos^2[(2N_x+1)kx] \times \exp\left[-\frac{((2\hbar kt/m)+z)^2}{2(\delta^2 + (\hbar^2 t^2/m^2\delta^2))}\right] \times \exp\left[-\frac{((2\hbar kt/m)+x)^2}{2(\delta^2 + (\hbar^2 t^2/m^2\delta^2))}\right].$$

From this, we can see that it is a two-dimensional interference pattern with Gaussian envelopes. Here $2t$ is the travel time from A to E.

One of the features of this result is the well-known free-space spreading of the wave packets, characterized by the doubling time $\tau_D = 2m\delta^2/\hbar$. The other feature is the shift in the envelope peak, in both x and z directions, at the rate of twice the recoil velocity, $2\hbar k/m \approx 12$ mm/s for ^{87}Rb. It is obvious from the expression that none of these two features affect the contrast of the fringes.

Fig. 4 shows a plot of this pattern for $\delta = 10$ nm and $2t = 30$ ns as a simple example. These numbers are completely arbitrary, and are chosen simply for graphical clarity, in order to ensure that both the fringe pattern and the roll-off are easily decipherable in the plot. Specifically, the choice of such a small value of t is made in order to keep it small compared to the doubling time of about 275 ns for this value of δ, and the choice of ^{87}Rb as the atom. A more realistic choice of parameters would be, for example, $\delta = 1$ mm, and $2t = 10$ ms. This will ensure the validity of our approximation that the interaction times are much smaller than the free evolution times. Note that the doubling time now is about 2750 s, and the wave packet spread would be completely negligible. However, in this case we will have nearly 10^{10} fringes within the envelope. Showing both the envelope and the fringes in the same graph would then be a difficult task. Since this is an analytical result, an interested reader can simply plot the fringe pattern for any given set of parameters within the constraints of the pulse parameters we have laid out in detail.

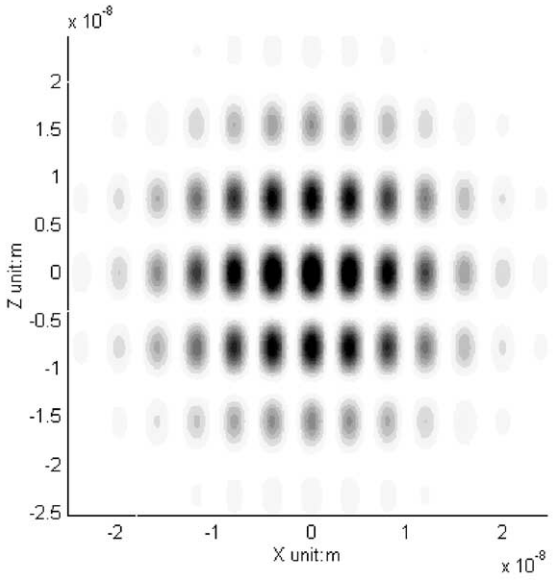

Fig. 4. A two-dimensional interference pattern after initial momentum averaging. This simulation assumes a 10 nm initial Gaussian wave packet size and total 60 ns propagation time.

In summary, we have proposed a scheme for a large angle interferometer using Raman pulses to produce a two-dimensional pattern with independent choice of grating spacings in each direction. This scheme may enable one to produce uniform arrays of structures such as quantum dots with characteristic sizes down to a few nanometers.

References

[1] T. Gustavson, P. Bouyer, M. Kasevich, Phys. Rev. Lett. 78 (1997) 2046.
[2] D. Keith, C. Ekstrom, Q. Turchette, D.E. Pritchard, Phys. Rev. Lett. 66 (1991) 2693.
[3] M.J. Snadden et al., Phys. Rev. Lett. 81 (1998) 971.
[4] D.S. Weiss, B.C. Young, S. Chu, Phys. Rev. Lett. 70 (1993) 2706.
[5] M.R. Andrews et al., Science 275 (1997) 637.
[6] P.L. Gould, G.A. Ruff, D.E. Pritchard, Phys. Rev. Lett. 56 (1986) 827.
[7] T. Pfau, C.S. Adams, J. Mlynek, Europhys. Lett. 21 (1993) 439.
[8] T. Pfau et al., Phys. Rev. Lett. 71 (1993) 3427.
[9] U. Janicke, M. Wilkens, Phys. Rev. A 50 (1994) 3265.

[10] P.R. Hemmer, M.S. Shahriar, M.G. Prentiss, D.P. Katz, K. Berggren, J. Mervis, N.P. Bigelow, Phys. Rev. Lett. 68 (1992) 3148.
[11] K.S. Johnson, A. Chu, T.W. Lynn, K.K. Berggren, M.S. Shahriar, M. Prentiss, Opt. Lett. 20 (1995) 1310.
[12] R. Grimm, J. Soding, Yu.B. Ovchinnikov, Opt. Lett. 19 (1994) 658.
[13] M.S. Shahriar, T. Zelevinsky, P.R. Hemmer. Available from http://xxx.lanl.gov/pdf/quant-ph/0007097.
[14] J.M. McGuirk, M.J. Snadden, M.A. Kasevich, Phys. Rev. Lett. 85 (2000) 4498.
[15] R. Younkin et al., Appl. Phys. Lett. 71 (1997) 1261.